*applied sciences*

MDPI

*Article*

# Design and Implementation of the AquaMIB Unmanned Surface Vehicle for Real-Time GIS-Based Spatial Interpolation and Autonomous Water Quality Monitoring

**Huseyin Duran [1,*] and Namık Kemal Sonmez [2]**

[1] Elmali Vocational School, Akdeniz University, 07700 Antalya, Türkiye
[2] Department of Space Science and Technologies, Faculty of Science, Akdeniz University, 07050 Antalya, Türkiye; nksonmez@akdeniz.edu.tr
* Correspondence: huseyinduran@akdeniz.edu.tr

## Featured Application

The AquaMIB system successfully performs accurate and continuous real-time water quality monitoring through autonomous navigation and online data transmission. By increasing sampling density, the system improves the representation of spatial variability, particularly demonstrating that Inverse Distance Weighting and Spline interpolation methods yield superior performance under limited data conditions. As a cost-effective and scalable decision-support tool, the system's real-time GIS-based mapping capabilities enable the early detection of environmental anomalies, thereby supporting the effective management of aquatic resources.

## Abstract

This article introduces the design and implementation of an Unmanned Surface Vehicle (USV), named "AquaMIB", which introduces a novel and integrated approach for real-time and autonomous water quality monitoring in aquatic environments. The system integrates modular hardware and software, combining sensors for temperature, pH, conductivity, dissolved oxygen, and oxidation reduction potential with GPS, LiDAR, a digital compass, communication modules, and a dedicated power unit. Software components include Python on a Raspberry Pi for navigation and control, C on an Atmega 324P for sensing, C++ on an Arduino Uno for remote control, and C#/JavaScript for the web-based control center. Users assign task points, and the USV autonomously navigates, collects data, and transmits it via RESTful API. Field trials showed 96.5% navigation accuracy over 2.2 km, with 66% of task points reached within 3 m. A total of 120 measurements were processed in real time and visualized as GIS-based spatial maps. The system demonstrates a cost-effective, modular solution for aquatic monitoring. The system's ability to generate real-time GIS maps enables immediate identification of environmental anomalies, transforming raw sensor data into an actionable decision-support tool for aquatic management.

**Keywords:** Unmanned Surface Vehicle (USV); AquaMIB; real-time water quality monitoring; GIS-based spatial analysis; obstacle detection

Check for updates

Academic Editor: Yutaka Ishibashi

Received: 6 January 2026
Revised: 21 January 2026
Accepted: 23 January 2026
Published: 24 January 2026

**Copyright:** © 2026 by the authors. Licensee MDPI, Basel, Switzerland. This article is an open access article distributed under the terms and conditions of the Creative Commons Attribution (CC BY) license.

## 1. Introduction

Water is an essential natural resource for human life, ecosystems, and all living species. Although about 71% of the Earth's surface is covered by water, only 2.5% is freshwater, and

just 0.3% of this freshwater is directly accessible in lakes, streams, and the atmosphere [1]. Combined with population growth, climate change, and industrialization, this limited availability highlights that access to clean water will become an increasingly critical environmental and social challenge. Therefore, continuous, real-time, and reliable monitoring of water quality is vital for the protection, sustainability, and effective management of water resources. Traditional monitoring methods, with limited measurement points and intervals, are often insufficient to capture sudden changes or the spatial distribution of contamination. To overcome these limitations, advanced techniques such as remote sensing [2], wireless sensor networks [3], and unmanned surface/underwater vehicles [4,5] are increasingly used.

An Unmanned Surface Vehicle (USV) is a vessel designed to operate without an onboard operator [6]. USVs can be remotely controlled or operate autonomously. They provide an effective solution for monitoring water parameters by supporting decision-making processes in detecting water quality and pollutants, while offering time and cost efficiency, especially in large or hard-to-reach areas.

The literature demonstrates significant interest in robotic systems and USV prototypes for water monitoring. In Nitte, India, a remote-controlled boat was designed to monitor real-time water characteristics and identify pollution zones, measuring parameters such as conductivity, pH, TDS, and temperature, and collecting samples for testing [7]. Xing et al. developed a USV for garbage recovery and turbidity monitoring [8]. Setiawan et al. [9] evaluated LoRa and 3DR telemetry for an autonomous sailboat in Indonesia. DeepChand et al. [10] created water quality index maps in Delhi using GIS. Yanes Luis et al. [11] compared Evolutionary Algorithms and Deep Reinforcement Learning for cyanobacteria detection in Paraguay. Other studies include accuracy tests of USV-based monitoring [12], mobile platforms for ecological research [13], robotic complexes for mining sites [14], and various low-cost USV prototypes for real-time monitoring [15–20]. These studies confirm that robotic platforms are increasingly adopted for diverse monitoring tasks.

Computer-aided data analysis and visualization tools, particularly GIS, play an important role in monitoring and managing aquatic environments. In many studies, thematic maps are created from water quality data collected by traditional methods, either from direct measurements or derived indices [10,21,22]. Interpolation methods are widely used to predict values in unmeasured areas and have been applied successfully in groundwater studies [23], rainfall estimation [24,25], and surface water quality analysis [26–28]. Studies include assessing Vibrio spread with Inverse Distance Weighting (IDW) [29], analyzing coastal water quality trends [30], and evaluating temperature and chlorophyll-A variations [31]. While IDW is widely used, it is sensitive to outliers and low sample density [32]. Kriging provides higher accuracy in many cases [33,34]. Spline methods successfully integrate river network structures [35], while the Natural Neighbor approach achieves reliable maps even with limited data [36]. Unlike previous studies that focus on single-point sampling, AquaMIB introduces a multi-container sampling system ($4 \times 200$ mL) integrated with real-time hybrid communication protocols (SignalR (version 9.0) and RESTful Application Programming Interface (API) ((HTTP/JSON-based))) for enhanced spatial representation.

Based on this background, the design and implementation of USVs for real-time, remote monitoring and mapping of water parameters is strongly recommended. In this study, a system is developed to generate areal distribution maps by integrating water parameter measurements with coordinates, sample collection, real-time visualization on a web-based panel, and interpolation techniques such as IDW, Kriging, Spline, and Natural Neighbor. The overall system, including the USV and the Water Parameter Measurement and Sampling Unit (WPMSU), is named AquaMIB.

This article is structured as follows: Section 1 introduces the context and research background; Section 2 presents the comprehensive architecture of the AquaMIB system, covering the design and implementation of the WPMSU, the USV, and the web-based control panel; Section 3 details the experimental results and data analysis; Section 4 discusses the technical evaluation, cost analysis, and system limitations;and Section 5 presents the conclusions and future directions..

## 2. Architecture of the AquaMIB System

In this study, a system called AquaMIB, composed of the WPMSU and the USV, was developed. For user interface and control, a dedicated remote controller and a web-based control panel were implemented (Figure 1). In the developed system, communication between the WPMSU and the USV, as well as between the remote controller and the USV, is established via ZigBee (XBee Series 2, Digi International, Hopkins, MN, USA), while communication between the USV and the website is maintained through 4G/LTE (SIM7600E, SIMCom Wireless Solutions, Shanghai, China). All communication within AquaMIB is designed to be bidirectional. In ZigBee communication, a star topology is used, where the USV is configured as the coordinator and the other devices function as routers.

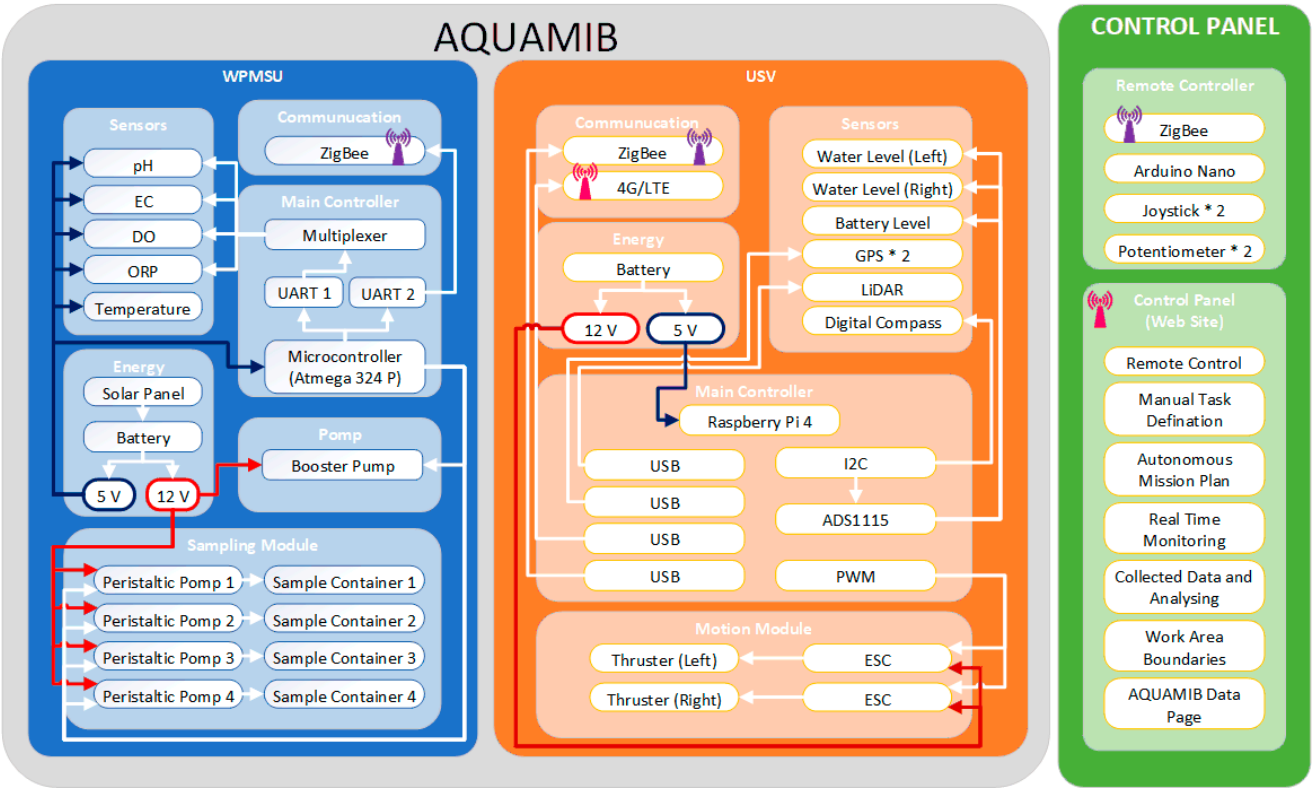


**Figure 1.** Block Diagram of the AquaMIB system.

### 2.1. Architecture of the WPMSU

The WPMSU (Figure 2a) consists of a main pipeline, control card (1), solar panel (2), battery (3), and a sampling system. The suction end of the main pipeline (4) includes sensors for oxidation reduction potential (ORP) (Atlas Scientific, Long Island City, NY, USA) (5), pH (Atlas Scientific, Long Island City, NY, USA) (6), dissolved oxygen (DO) (Atlas Scientific, Long Island City, NY, USA) (7), electrical conductivity (EC) (Atlas Scientific, Long Island City, NY, USA) (8), and temperature (DS18B20, Maxim Integrated, San Jose, CA, USA) (9). Additional components are the sample system connection (10), pump (11), and discharge section (12), which together enable the measurement of water parameters and

take sample. In the sampling system, each hose connected to the main pipeline is routed to the peristaltic pumps (13) and subsequently to the sample containers (14), as illustrated in Figure 2b.

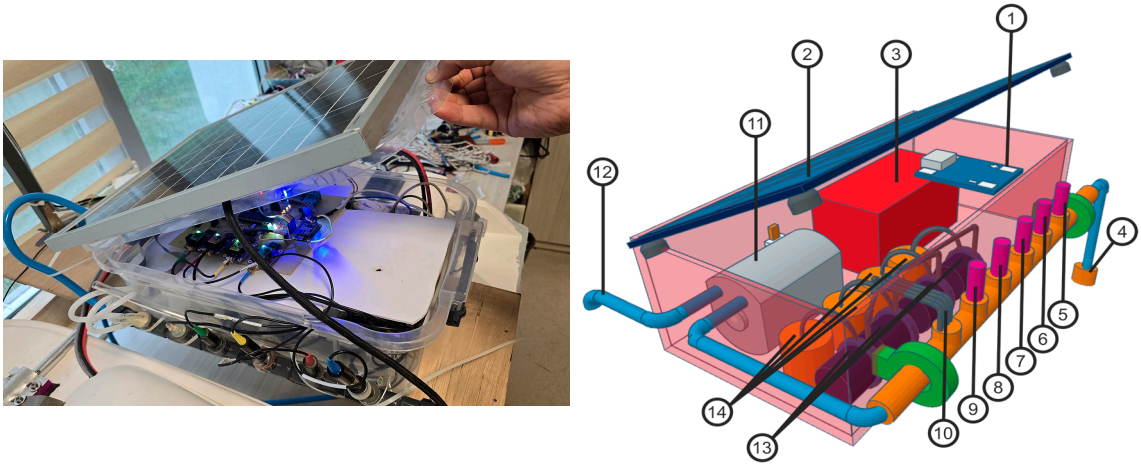


(**a**) (**b**)

**Figure 2.** WPMSU perspective view (**a**) Photo; (**b**) CAD model.

The unit draws water from its location into the main pipeline with the help of a pump, either while the USV is in motion or stationary. Water quality parameters are measured using ORP, pH, DO, EC, and temperature sensors. The system can also collect samples when necessary and subsequently discharges the water in the pipeline. These types of sensors are widely reported in the literature and are commonly used in surface water quality monitoring to assess water quality. All sensors employed in the system were calibrated using standard buffer solutions in accordance with the manufacturer's instructions during the development phase and prior to field experiments to ensure measurement accuracy. Technical specifications of the sensors employed in the unit are presented in Table 1.

**Table 1.** Specifications of the water sensors used in the WPMSU.

| Sensor | Measurement Range | Resolution | Accuracy (±) | Output Signal |
|---|---|---|---|---|
| Temperature | –55–125 °C | 0.1 °C | 0.5 °C | Analog |
| pH | 0–14 pH | 0.001 pH | 0.002 pH | |
| EC | 5–200,000 µS/cm | <99 → 0.01 µS/cm<br><999 → 0.1 µS/cm<br><9999 → 1 µS/cm<br><99 999 → 10 µS/cm<br><999 999 → 100 µS/cm | 2% | Digital |
| DO | 0–100 mg/L | — | 0.05 mg/L | |
| ORP | –1019.9 mV<br>+1019.9 mV | — | 0.1 mV | |

The unit can operate either autonomously or manually. In manual mode, individual operations such as reading parameter values, starting or stopping the motors, and performing sampling can be carried out separately. In autonomous mode, all parameter values are read sequentially, and the required sampling is performed automatically. At the end of both modes, the system returns values (e.g., motor status, temperature readings) are transmitted to the control panel, where logging operations are carried out. The algorithm describing the workflow of the unit is presented in Figure 3.

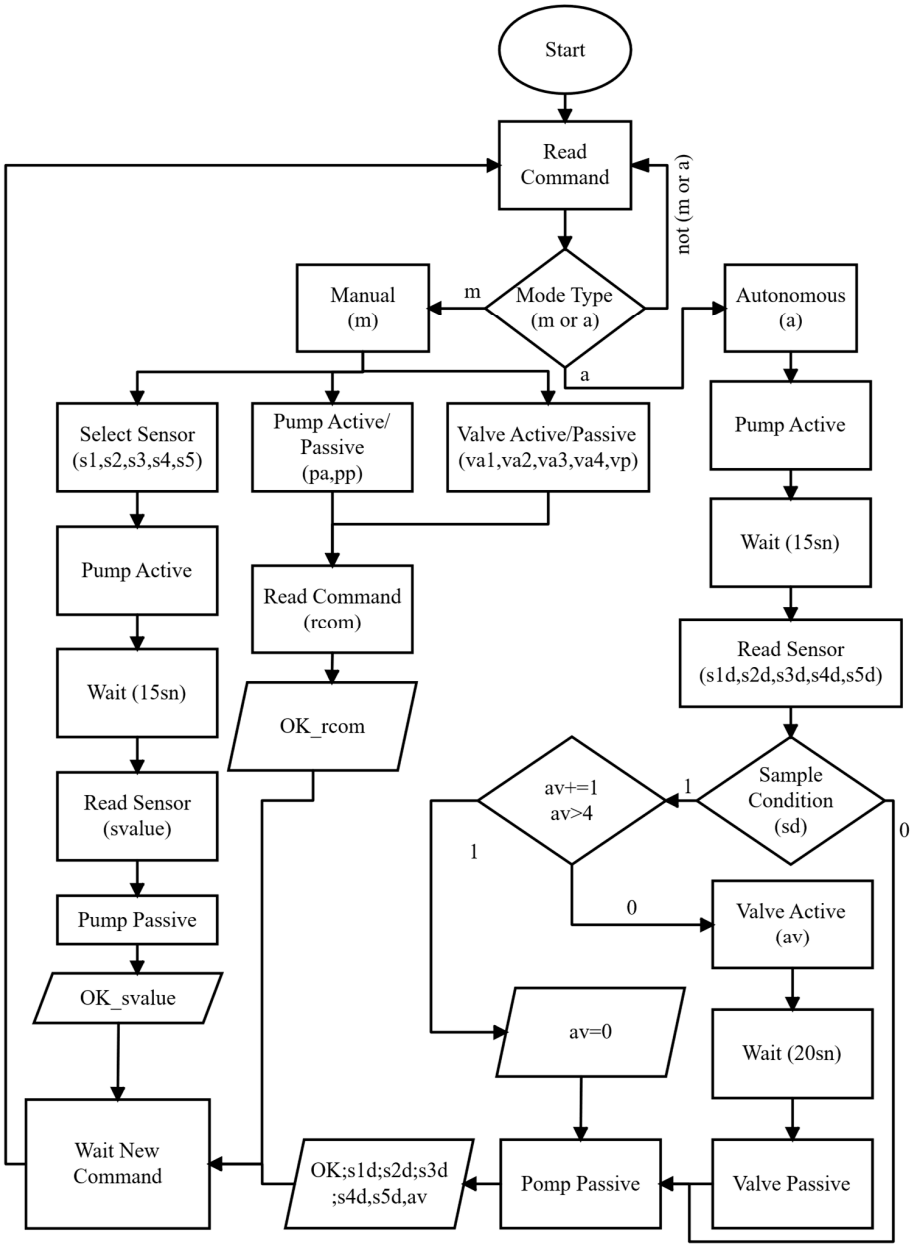


**Figure 3.** WPMSU software algorithm.

To transfer water to the main pipeline, the booster pump operates for 15 s before the reading process. This duration is determined by the time required for water to enter through the suction head and exit the discharge section. The pump is positioned at the end of the pipeline to prevent changes in water parameters within the system. To avoid air intake during operation and leakage in the pipeline, pressure-resistant gaskets are used for the assembly of sensors and hoses. In addition, a strainer is placed at the suction tip to prevent substances that could damage the pump and sensors from being absorbed.

During sensor readings, meaningless data were occasionally observed. Since this causes incorrect measurements, each parameter is recorded at 100 ms intervals until 50 valid values are obtained, and then the average is calculated. Kawahito and Seo [37] proposed this averaging method to obtain reliable sensor data. According to their studies five parameters can be measured in approximately 25 s. Tests with different reading intervals and sample sizes showed that excessive repetitions caused time loss, whereas fewer readings resulted in data loss.

In the sampling system, four 200 mL containers are used. However, filling them completely may lead to overflow due to USV movement. Therefore, the filling volume is limited to 80–100 mL, and it was determined that 20 s of peristaltic pump operation is sufficient to collect this amount. For comparison, Chang et al. [38] used two 60 mL containers in their USV, while Arko et al. [39] used a single 100 mL container. The developed system is distinctive compared to these studies in terms of both the number of samples collected and the total volume.

### 2.2. Architecture of the USV

The USV is designed to transport the WPMSU to designated points on the water surface according to commands received from the control center. It can operate either autonomously or manually. The configuration of the USV is determined by the hull design and the optimal placement of its components, while its technical specifications are presented in Table 2.

**Table 2.** General specifications of the USV.

| Specification | Value |
|---|---|
| Total length | 1.0 m |
| Total width | 0.9 m |
| Total height | 0.9 m |
| Energy | 24 Ah Lithium Polymer |
| Battery life | 3 h |
| Payload | 15 kg |
| Material | Fiberglass, aluminum, and waterproof chipboard |
| Weight | 20 kg |
| Remote range | Global System for Mobile Communications (GSM) (service provider coverage area); ZigBee (<3 km) |
| Speed | 1.25 m/s |

Although different design types exist for surface vehicles used in water parameter monitoring, the catamaran form is the most widely preferred. In this study, the USV was developed in a catamaran configuration and its main structural components are shown in Figure 4a. Figure 4b shows the CAD design, highlighting the two fiberglass hulls, aluminum frame, waterproof payload platform, and mast equipped with antennas, LiDAR (RPLIDAR A1, Slamtec, Shanghai, China) , GPS (NEO-6M, u-blox, Thalwil, Switzerland), and a digital compass(HMC5883L, Honeywell, Charlotte, NC, USA) .

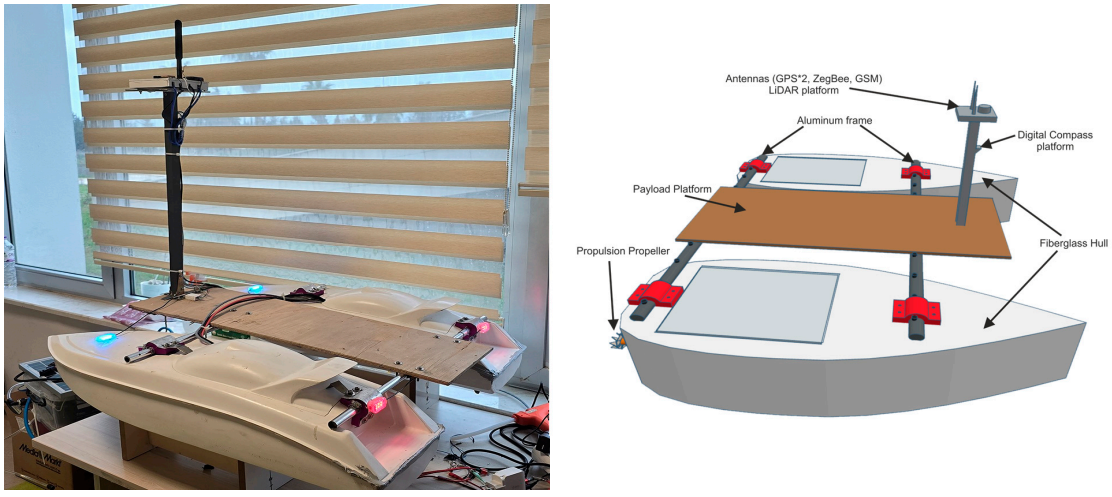


(**a**) (**b**)

**Figure 4.** USV perspective view (**a**) prototype photo; (**b**) CAD design.

#### 2.2.1. USV Design

The hull of the USV consists of two V-bottom fiberglass shells, each measuring 100 cm in length and 36 cm in width. The two hulls are positioned parallel to each other with a spacing of 45 cm and are connected at the bow and stern by corrosion-resistant aluminum profiles. An 80 cm by 35 cm water-resistant wooden platform is mounted on these profiles to carry the WPMSU. This platform is also designed to accommodate additional hardware such as cameras or robotic arms in future studies. At the front of the platform, a 60 cm high aluminum mast is installed to support antennas for communication and positioning systems. Furthermore, red lights are integrated at the stern and blue lights at the bow to improve visibility on the water, enhance safety, and indicate the orientation of the USV.

#### 2.2.2. USV Motion System

The motion system consists of the equipment used to propel the USV from one point to another on the water surface. Each hull is equipped with a motor, shaft, and propeller. Brushed motors are employed to provide the required thrust, delivering high torque and reaching up to 15,000 RPM. Each motor is controlled by a waterproof 60 A electronic speed controller, which enables bidirectional rotation. The rotational motion is transmitted to the propellers through shafts. The propellers are three-blade torque types with a diameter of 80 mm, mounted to rotate in opposite directions on each side of the USV. When both motors rotate clockwise, the USV moves forward; when they rotate counterclockwise, it moves backward. By varying the relative speeds and directions of the motors, steering is achieved without the need for rudders.

Although identical hardware is used for both hulls, deviations were observed when the same Pulse Width Modulation (PWM) signal was applied to each motor. Wang et al. [40] solved this issue by applying the same DC supply to each motor and compensating with custom PWM adjustments. A similar approach is adopted in this study: motor speeds are mapped to USV-specific values determined by software, and distinct PWM values are assigned to each motor. These values range from 7 to 20 in the control algorithm, instead of representing actual physical speeds. A value of 10 stops the motors, values of 7–9 drive the USV backward, and values of 11–20 drive it forward. For example, when both motors receive the command (15, 15), the USV moves straight ahead without deviation.

The USV can be operated remotely and cruise autonomously. For remote operation, two types of control interfaces were developed: a physical controller (Figure 5a) and a web-based controller (Figure 5b). Communication with the physical controller is handled via ZigBee, while the web-based interface communicates through SignalR. In both cases, speed values are transmitted to the USV every second.

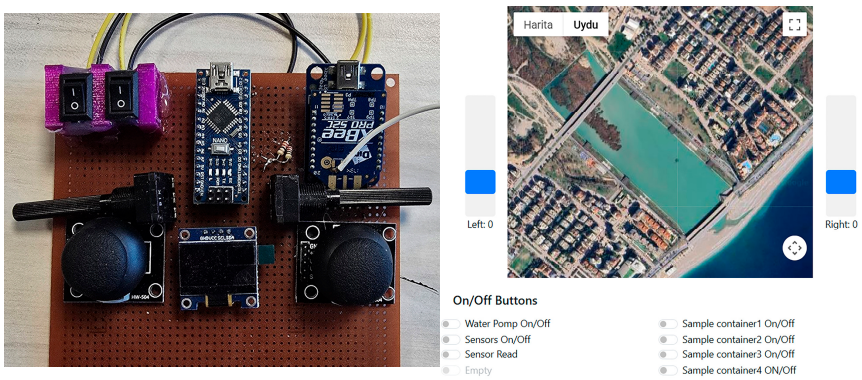


(**a**) (**b**)

**Figure 5.** Remote control units (**a**) physical; (**b**) Web-based.

2.2.3. USV Electronic Design

The hardware architecture is divided into subsystems or modules, as shown in Figure 1. The USV control unit is the central component that manages the operation of the entire system, including motion and direction control, data acquisition from positioning systems, communication with the WPMSU, and remote-control integration. A Raspberry Pi 4 (Raspberry Pi Foundation, Cambridge, UK) minicomputer is used for these operations. The system software is developed on the Raspberry Pi using the Linux (64-bit, Debian-based Linux, version 12)mvc operating system and the Python (version 3.10) programming language. The USV's hardware connected to the USB ports has been assigned fixed addresses with the udev rules in Linux, ensuring consistency at every boot.

The system is built on a multi-threading mechanism, where different processes are executed simultaneously through independent threads. Villa et al. [41] state in their study that this architecture enables the system to operate with high performance and low latency. At the same time, the threads can be executed according to their priority. For example, there is a prioritization structure for control commands: the physical controller has the highest priority, the web-based controller has the second priority, and the data from the autonomous driving algorithm has the lowest priority. In this way, immediate interventions can be made during autonomous driving.

Energy is supplied by two Lithium Polymer batteries, each with a capacity of 12 Volts and 12 Ah. To ensure weight balance, each battery is placed in a separate shell, and the batteries are connected in parallel to balance energy consumption. While the motion system is directly supplied with a voltage of 12 V, the Raspberry Pi, GPS, and similar low-voltage components operate with 5 V supplied through a voltage regulator. To monitor the battery capacity, a connection is established with the Raspberry Pi via an ADS1115 (Texas Instruments, Dallas, TX, USA) analog-to-digital converter module, enabling real-time capacity information to be transferred to the control panel. In addition, water level sensors placed in each hull are connected to the ADS1115 module to monitor potential water leaks, and this information can also be displayed via the control panel.

The USV's positioning system uses two GPS modules to determine the vehicle's position on the water surface, a digital compass for its orientation, and a LiDAR sensor to detect environmental obstacles. The LiDAR has a scanning rate of 5–13 Hz and a maximum detection range of 12 m. It performs 360° 2D omnidirectional laser distance measurement and obstacle detection by sampling 8000 points per second. The LiDAR data is divided and filtered into five different regions: front, right front, left front, right rear, and left rear, to determine the direction and intensity of obstacles, as illustrated in Figure 6.

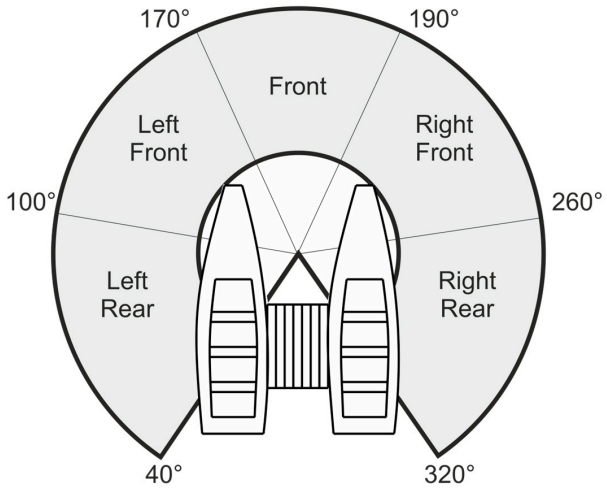


**Figure 6.** LiDAR data division regions.

With the LiDAR, which can perform 10 rotations per second and capture approximately 450–600 data points in each rotation, an average of about 5000 data points can be obtained every second. Invalid data are filtered out from the incoming dataset. In addition, values less than 300 mm and greater than 5000 mm obtained from the LiDAR are excluded from the evaluation. After these procedures, only the data between angular ranges of 40°–320° are considered significant. The reason for this is that the 180° angle of the LiDAR corresponds to the front of the USV, while the 320°–360° and 0–40° sectors correspond to the rear of the USV.

Obstacle detection is determined according to the density of objects in partial areas. To evaluate density, a structure has been developed that prioritizes regions from the most important to the least important: the front, the right/left front, and finally the right/left rear. In this structure, the front is assigned a weight of 1.0, the sides 0.7, and the rear 0.4. In addition, both the distance and the density of the obstacles are evaluated with a separate calculation.

For density evaluation, the densest areas are assigned a weight of 1.0, while sparse areas are assigned a weight of 0. Intermediate values correspond to regions of medium density. The density values for each region of the USV are calculated according to the following formula:

$$Y_i = \sum_{j \in region_i} \omega_\theta(\theta_j) \times \frac{d_{max} - d_j}{d_{max} - d_{min}} \quad (1)$$

In the formula, $Y_i$ shows the total obstacle density of the region, $j$ represents an obstacle detected in the area, $\omega_\theta$ is the weight of the obstacle angle, $\theta_j$ is the angle of the obstacle, and $d_j$ is the distance of the obstacle.

Speed data are sent to the motors so that the USV can turn toward the side where the obstacle density is low. The process of reading and analyzing LiDAR data, and sending signals to the motors, is defined as a stand-alone thread and is automatically activated during autonomous driving.

GPS data are the most critical source for determining the USV's position on the water. Two separate location datasets are obtained from the GSM module and the GPS module. Both incoming datasets are merged into a single output using the calculation described below for error correction and accuracy improvement.

$$If \left| d_{gpsp} - d_{gpse} \right| > 3m \rightarrow P_{gps} isoutlier \quad (2)$$

$$If \left| d_{gsmp} - d_{gsme} \right| > 3m \rightarrow P_{gsm} isoutlier \quad (3)$$

$$P = \begin{cases} \left( \frac{lat_{gsm} + lat_{gps}}{2}, \frac{lon_{gsm} + lon_{gps}}{2} \right) & if\ both\ valid\ or\ invalid \\ (lat_{gsm}, lon_{gsm}) & if\ only\ P_{gsm}\ valid \\ (lat_{gps}, lon_{gps}) & if\ only\ P_{gps}\ valid \end{cases} \quad (4)$$

In the proposed position fusion approach, $d_{gpsp}$ and $d_{gpse}$ represent the positional differences between consecutive measurements obtained from the GPS module and the GSM-based positioning system, respectively. These distance values are used to detect abnormal deviations caused by temporary signal degradation or measurement noise. A threshold value of 3 m is empirically selected to identify unreliable position updates and mark them as outliers.

The parameter $P$ denotes the final estimated position of the USV. If both positioning sources are valid or invalid, the estimated position is computed as the average of the two measurements. If only one source is considered valid, the position estimate relies solely on that source. This adaptive selection strategy improves positional robustness and reduces the impact of sporadic positioning errors.

The USV's communication system is designed to support bidirectional operations such as the export of collected data, the transmission of remote commands, and the retrieval of data. Two different communication protocols are employed in this system. The ZigBee protocol is used for communication with the WPMSU and for physical controller. For long-distance communication, a GSM module supporting 4G is utilized. This module enables communication between the USV and the web-based control panel, as well as the automatic connection of the Raspberry Pi to the Internet. The Point-to-Point Protocol (PPP) method is applied to establish the Internet connection. For the PPP method, a ppp-peer file is created, and an initialization script is prepared. The connection is configured to start automatically each time the Raspberry Pi is powered on. The USV cannot be activated without an Internet connection.

Feedback control systems enable dynamic variables such as direction and speed to be managed precisely in autonomous vehicles. Control of the USV requires a delicate balance against environmental disturbances and system inertia. During autonomous navigation, the USV's instantaneous position is determined by latitude and longitude data from GPS sensors, while its orientation is measured using a digital compass. The linear distance between the current position of the USV and the target position is calculated using the Haversine formula. At the same time, the heading angle to the target is normalized within the range of 0°–360°, based on geographical coordinates.

To ensure that the AquaMIB follows the desired path, traditional PID control logic is applied for both speed and heading. The PID controller continuously calculates the error between the current system state and the target value and generates motor commands based on this error signal. In heading control, the difference between the target direction and the current direction is defined as the error. This error is provided as input to the PID controller, which produces a control signal that generates differential thrust. The proportional gain $K_{p,x}$ determines the immediate response of the system to the heading error and directly affects the turning aggressiveness of the vehicle. The integral gain $K_{i,x}$ compensates for accumulated steady-state errors caused by persistent environmental disturbances such as wind and surface currents. The derivative gain $K_{d,x}$ acts as a damping term by suppressing rapid changes in the error signal, thereby improving system stability and reducing oscillations. For heading ($x = \psi$) and speed ($x = u$), PID equations are used as follows:

$$u_x(t) = K_{p,x}\, e_x + K_{i,x} \int e_x(t)dt + K_{d,x} \frac{de_x(t)}{dt} \tag{5}$$

The values $u_\psi$ and $u_u$ obtained from both controllers are used to calculate the commands applied to the vehicle's two engines. The parameter $k_{rotation}$ scales the differential thrust applied between the left and right motors and thus determines the turning sensitivity of the vehicle. According to the principle of differential thrust, the right and left engine commands are defined as:

$$u_L = u_u + k_{rotation}.u_\psi \tag{6}$$

$$u_R = u_u - k_{rotation}.u_\psi \tag{7}$$

All control parameters were tuned experimentally using a trial-and-error approach. Since heading stability is the primary factor determining navigation accuracy, the tuning process focused on the heading controller parameters. In the experimental setup, the control gains were set to $K_{p,\psi} = 0.8$, $K_{i,\psi} = 0.05$, $K_{d,\psi} = 0.2$, and $k_{rotation} = 0.6$. The parameter $k_{rotation}$ acts as a scaling factor that maps the heading control output to the differential thrust applied to the left and right motors. These experimentally determined values provided robust navigation under moderate environmental conditions. However, minor deviations were observed during sharp turns (as detailed in Section 3). These results indicate that the fixed-gain controller has sensitivity limitations when facing strong lateral disturbances,

such as wind and currents. Thanks to the PID controller, the boat moves at the targeted speed and in the correct direction. At the same time, due to the use of differential thrust, steering can be achieved without the need for a rudder mechanism. Figure 7 illustrates the orientation and positions of the vehicle at three different time moments: red ($t_1$), blue ($t_2$), and green ($t_3$). In this way, the temporal progression of the directional error and the corrective effect of the PID controller can be monitored.

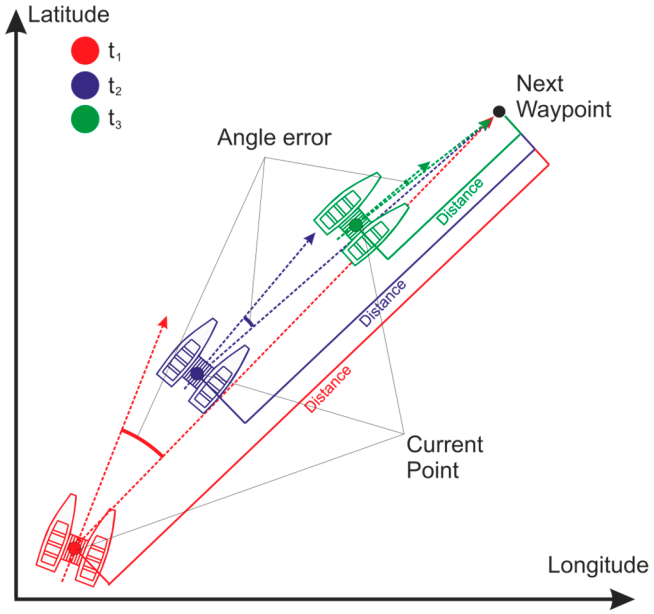


**Figure 7.** Effect of PID algorithm on distance and angle of error.

Autonomous tasks are transmitted from the control panel to USV. The incoming task list is stored in a newly created Comma-Separated Values (CSV) file, which includes the target coordinates, mission parameters, and time information. The time information is recorded when each mission starts and updated once the vehicle reaches its destination. If the vehicle does not approach the target within 3 m, it continues moving forward. When the destination is reached, a command is sent to the WPMSU, and the received data packet is processed. These data are appended to the task list and transmitted to the control center via the Raspberry Pi through an API. The data, sent in JSON format, are also stored in the task file together with the task status and completion time. Subsequently, the next task is initiated. Once all tasks have been completed, USV returns to the home point (Figure 8).

The USV sends information such as battery status, water level, position, direction, and motor speeds from the Raspberry Pi to the control center using SignalR. Thanks to asynchronous data transmission, uninterrupted and stable operation of the system is ensured, instant updates are transferred without delay. This structure makes it possible for the vehicle to react quickly to environmental variables and to monitor it in real time.

### *2.3. Web-Based Control Panel*

The control panel is a comprehensive web-based interface designed for the remote control and monitoring of the AquaMIB system, as well as for the analysis of collected data. It serves as a central platform where AquaMIB operational processes are managed, supervised, and analyzed.

The technical infrastructure of the control panel adopts a hybrid approach that combines modern web technologies with real-time data communication methods. The panel is built on the ASP.NET Core MVC (version 9.0, Microsoft) architecture with C# (version 10.0). A responsive and interactive structure is achieved by using HTML5, CSS3, and JavaScript

(ES6 standard) for user interface design. SignalR technology is employed to instantly update data transmitted from AquaMIB and deliver it to the user, while a RESTful API infrastructure is used for database operations and the transfer of larger or more detailed datasets. For map-based visualization and geographical analysis, the Google Maps (version 3) API is integrated.

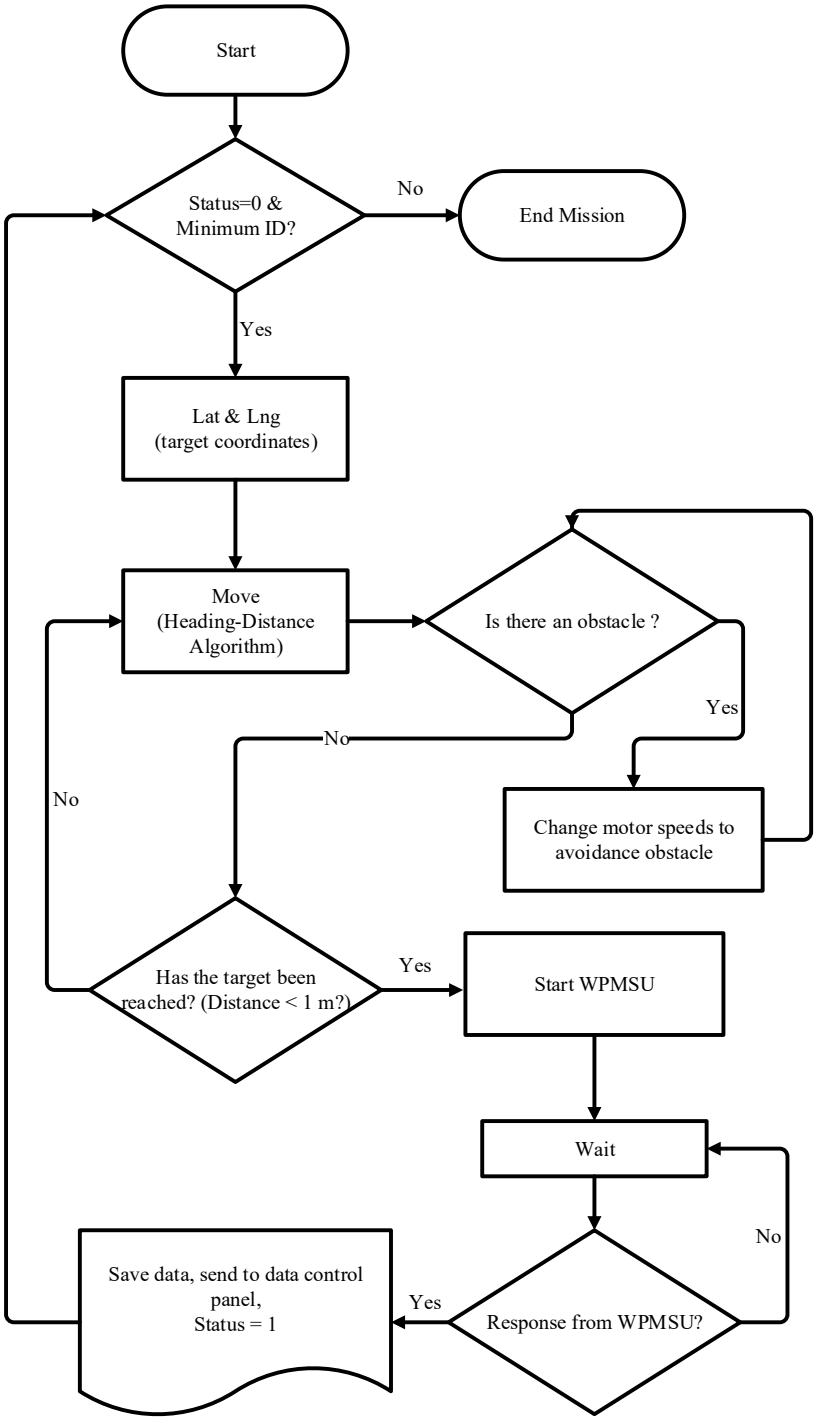


**Figure 8.** AquaMIB autonomous operation algorithm.

The control panel provides a versatile interface that supports a wide range of functionalities, including the definition of autonomous tasks either manually or spatially, real-time monitoring of missions, remote-control operations, and analysis of collected data. The system also enables downloading of acquired data in CSV format and the generation of

real-time areal distribution maps by applying interpolation methods such as IDW, Kriging, Spline, and Natural Neighbor.

In autonomous task definitions, the user can select coordinates individually or define a region according to the number of monitoring points. For areal selections, once a region is specified, the number of points is determined and a homogeneous, systematic grid structure is created so that all points fall within the selected area [42]. For energy efficiency, the AquaMIB path is optimized by applying the zigzag sorting method. The user can also specify resolution values for areal monitoring and manually remove unwanted points from the task list. This hybrid strategy combines areal scanning and manual coordinate selection approaches described in the literature, allowing AquaMIB to perform such operations in real time.

The panel also offers mission management and real-time monitoring of AquaMIB. Tasks saved in the system are listed, and operations such as starting, stopping, and pausing tasks can be controlled on this page. The current position of AquaMIB, engine speeds, safety information (such as water level in shells and battery status), and all operational steps can be monitored in real time. For this purpose, SignalR technology ensures that critical information is transmitted from AquaMIB to the control unit every second, while less critical or larger datasets are sent via the RESTful API with a delay of approximately 3 s. This hybrid communication approach enables the system to operate flexibly, ensuring both instantaneous responsiveness and efficient high-volume data transfer.

Remote control of AquaMIB is another important feature of the panel. In this mode, the motor speeds can be adjusted, and the pump, sensors, and sampling system can be activated or deactivated. The physical controller offers a range of up to 3 km, while the web-based controller allows operation from anywhere with Internet access. Compared to limited-range solutions such as Wi-Fi [43] or Bluetooth [38], this dual system ensures seamless and reliable data transfer both locally and remotely, offering superior communication flexibility and range. As a result, data are transmitted through two different communication systems with two independent remote-control mechanisms.

The control panel also supports the listing and downloading of collected water parameter data. The collected values can be queried for specific date ranges, and the resulting datasets can be saved in CSV format for further analysis. Through the integrated GIS infrastructure, areal distribution maps of collected water quality parameters (EC, temperature, pH, DO, ORP) can be generated. These maps are produced and analyzed in real time using different interpolation methods such as IDW [44], Kriging [45], Spline [46], and Natural Neighbor [47]. In this way, estimated values in unmeasured areas are obtained, providing a spatial representation of water quality. Furthermore, heat maps can be created on the online map to visualize parameter values in real time. This real-time analysis capability provides a significant advantage for detecting sudden changes and enabling rapid interventions.

Finally, the control panel allows the user to define operational boundaries for AquaMIB. This feature prevents the vehicle from moving beyond predefined limits in cases such as signal loss or loss of control, offering an additional layer of safety and enhancing the robustness of the AquaMIB system compared with other studies in the literature.

## 3. Experiment Results and Analysis

AquaMIB can operate in both autonomous and manual control modes. Before executing tasks in autonomous mode, critical performance parameters such as speed, orientation, deflection, and obstacle avoidance are evaluated under manual control conditions. The steering functions and hardware inspection capabilities of both the remote controller and the web-based controller are tested in a controlled pool environment (Figure 9).



**Figure 9.** AquaMIB pool tests.

During the experiments, the effects of varying engine speed values on the forward motion and turning performance of AquaMIB are observed. The position of the WPMSU on the USV is adjusted to ensure that the equipment is balanced precisely at the midpoint of the vehicle. In this way, deviations caused by weight imbalance are effectively minimized.

After all hardware components are successfully tested in the pool environment, autonomous driving experiments are conducted (Figure 10). These experiments are carried out in the Bogacayi region of Antalya. For the autonomous mode tests, four different mission plans are prepared. Plans 1 and 2 are generated by manually selecting individual coordinates, whereas Plans 3 and 4 are designed based on spatial field selection.



**Figure 10.** AquaMIB autonomous works.

First, all mission plans are configured sequentially on the control panel. In Plan 1, two coordinate points are selected on the map, and the option of not taking samples between these two points is enabled. In Plan 2, three coordinate points are marked, and the sampling option is activated for the third coordinate point.

For Plan 3 and Plan 4, spatial field selection is applied within the coordinate boundaries (36.852471, 30.624705–36.853776, 30.626249–36.856643, 30.622258–36.855287, 30.620821). As a result, 5 and 15 measurement points are generated for Plans 3 and 4, respectively. During the registration phase of Plan 4, the 14th measurement point is removed because it coincided with a reed-covered area, leaving a total of 14 valid points. The measurement points and their execution sequences for all plans are monitored on the control panel (Figure 11).




**Figure 11.** Routes identified (**a**) Plan 1; (**b**) Plan 2; (**c**) Plan 3; (**d**) Plan 4.

In Plan 1, the distance between the two selected coordinates is approximately 145 m, and the mission is completed within 5 min and 31 s after initiation. While the travel between the two coordinates takes 2 min and 30 s, the remaining 3 min and 1 s are spent reading parameter values, transmitting them to the server, and recording them in the database.

Plan 2 consists of three coordinate points, with a total route length of 261 m. AquaMIB completes this mission in 10 min and 8 s. Of this duration, 6 min and 6 s are dedicated to measurements and sampling, while the remaining 4 min and 2 s are spent on navigation. Water sampling is performed at the last coordinate point in Plan 2. For this task, the peristaltic pump operates for 20 s to collect enough water, which is then transferred to the sample container. The final state of the sample container following this process is shown in Figure 12.



**Figure 12.** Sample container and collected water.

Plan 3 consists of 5 coordinate points, with a total route length of 591.53 m. The tasks defined in this plan take 20 min and 31 s to complete. Of this duration, 11 min and 25 s

correspond to the measurement of water parameter values, while 9 min and 6 s are spent navigating between points.

Plan 4 includes 14 coordinate points, with a total calculated distance of 1170.1 m. The measurement of water parameters at these 14 points requires 23 min and 9 s, while 18 min and 58 s are spent traveling between points. The total mission time for Plan 4 is therefore 42 min and 7 s.

During the execution of these plans, AquaMIB is monitored in real time via the control panel, and information such as position and speed is recorded in the database. The path followed by AquaMIB for each plan are illustrated in Figure 13 in red.




**Figure 13.** AquaMIB road route and linear route (**a**) Plan 1; (**b**) Plan 2; (**c**) Plan 3; (**d**) Plan 4.

In autonomous mode, the operational area was bounded by high walls and shoreline obstacles. During the field trials covering a total autonomous navigation distance of 2248.35 m, the obstacle avoidance system demonstrated success rate, with zero collisions recorded. The density-weighting algorithm allowed the AquaMIB to consistently maintain a minimum safety clearance of approximately 1.5 m from the walls (Points 1, 7, and 8 in Plan 4), effectively validating the system's operational safety without the need for simple threshold-based emergency stops. Differences between the actual trajectory of AquaMIB and the ideal linear route are observed in all four autonomous plans. These deviations between the path followed by AquaMIB and the straight-line route are illustrated in Figure 14.

In Plan 1, although the linear route distance between the two points is 145 m, the actual path traveled by AquaMIB is 174.87 m, indicating an approximate 20.6% increase in distance. This deviation is attributed to improper maneuvers along the route, preventing the vehicle from moving directly toward the target. In Plan 2, the linear distance between the three coordinates is 261.28 m, whereas the actual path followed is 265.58 m. The difference here is relatively small, amounting to only 1.6%. This suggests that the vessel followed the intended course efficiently, remaining close to the direct line to the target. Plan 3 includes five coordinate points. The linear route distance among these points is 591.53 m, while the path followed is 600.14 m. The resulting difference of 1.45% is very small, demonstrating that the route tracking accuracy in this plan is also quite high. In Plan

4, the linear route is calculated as 1170.1 m, whereas the actual traveled path is 1196.67 m. The deviation of 2.27% is slightly higher than in the other plans, yet overall the route is still followed directly and efficiently.

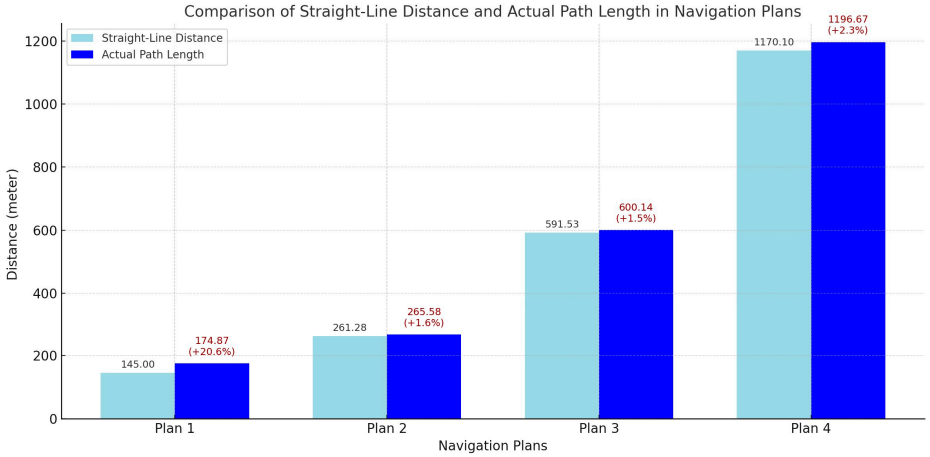


**Figure 14.** Linear distance and AquaMIB route for Plans 1–4.

Among all plans, the largest deviation is observed in Plan 1. The reason is the relatively long distance between consecutive coordinates, which amplifies the effect of corrective maneuvers. In the other plans, course deviations remain at a very low level. These results demonstrate that the system is generally successful in moving directly to the targets and that route optimization is effectively achieved. During the execution of the plans, not only the paths followed by AquaMIB but also the differences between the task points defined on the control panel and the coordinates where water parameters are recorded are analyzed (Figure 15).

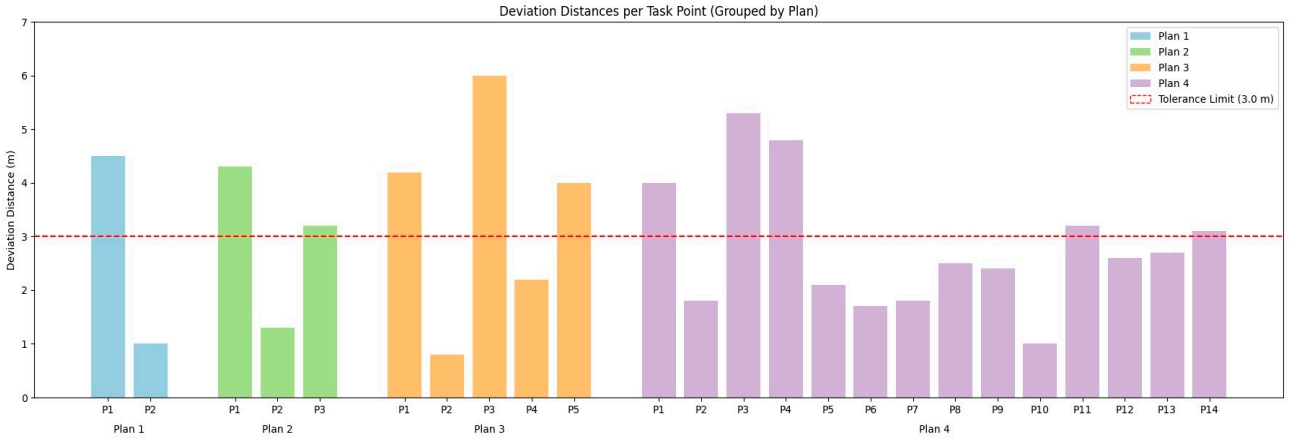


**Figure 15.** Distance differences between the target coordinate and the measured coordinate in 4 different planes.

Standard error-based metrics were calculated from distance deviation data to measure average tracking accuracy. Since the number of duty points differed among the navigation plans, normalized metrics (NIAE and NITAE) were used, dividing the cumulative error values by the respective number of duty points, to ensure a fair comparison. The resulting metrics, summarized in Table 3, show significant differences in movement behavior among the navigation plans. Plans 1 and 2 show lower average errors, while Plan 3 shows larger deviations, as reflected by higher MAE and RMSE values. The relatively higher normalized

cumulative error observed in Plan 4 suggests that, despite the lower average error, small tracking deviations persist for a longer period.

**Table 3.** Tracking error metrics for different navigation plans..

| Plan | MAE (m) | RMSE (m) | NIAE | NITAE |
|---|---|---|---|---|
| Plan 1 | 2.75 | 3.26 | 2.75 | 3.25 |
| Plan 2 | 2.93 | 3.18 | 2.93 | 5.50 |
| Plan 3 | 3.44 | 3.88 | 3.44 | 10.52 |
| Plan 4 | 2.79 | 3.02 | 2.79 | 19.46 |

Within the scope of each plan, the distance differences between the targeted task point and the point where AquaMIB records measurements and collects samples are evaluated using a tolerance limit of 3 m [48]. In Plan 1, two task points are measured. At Point 1, the deviation exceeds the tolerance limit with a value of 4.55 m, whereas at Point 2 the deviation remains below the tolerance with 1.11 m. In Plan 2, three task points are evaluated. At Point 1, the tolerance is exceeded with 4.34 m, while at Point 2 the deviation is 1.45 m and at Point 3 it is 3.22 m, remaining at or just below the threshold. The fact that the deviation is slightly above the tolerance, particularly at Point 3, indicates the need for greater maneuvering precision. Plan 3 consists of five task points. Significant deviations are observed at certain points, such as Points 1, 3, and 5. However, at Points 2 and 4, the deviations remain within the 2–3 m range, demonstrating more controlled movement. Plan 4 covers the largest number of task points. In this plan, most deviations found to be below the 3 m tolerance limit. Nevertheless, it is noteworthy that at some points (Points 1, 3, 4, 11, and 14), the tolerance limit is exceeded. The 3 m tolerance exceedance observed at specific points (e.g., Point 1 in Plan 1) is likely due to the initial acceleration phase and cumulative PID error at sharp turning angles, which will be addressed by integrating RTK-GNSS in future iterations.

Overall, the evaluation demonstrates that although minor deviations are inevitable due to environmental and operational factors, AquaMIB generally operates within the defined tolerance limits. These results confirm that the system can achieve reliable positional accuracy in most operational scenarios. In this study, water quality data are also collected under four different mission plans on the same day within an area of approximately 10 ha (Table 4).

Plans 1, 2, 3, and 4 are conducted with increasing spatial density, by measuring from 2, 3, 5, and 14 different points, respectively. Overall, the temperature values remain nearly constant across all plans, indicating the homogeneity of daytime environmental conditions.

EC values exhibit the highest average in Plan 1, while relatively lower but more stable values are observed in the subsequent plans. This suggests that although dissolved ion differences occur intermittently in the field, these variations become more evenly distributed as the number of sampling points increases.

When the pH, DO, and ORP parameters are evaluated, it is evident that the natural variability in the study area is captured more clearly with higher sampling density. Plan 4 reveals significant differences in pH and ORP values at certain points. This demonstrates that low-density sampling plans may overlook micro-scale variations in the field, whereas high-density plans provide opportunities for more detailed analysis.

With respect to DO, all plans yield relatively stable values of approximately 5 mg/L. In conclusion, this multi-stage sampling design within the same area highlights the critical role of data density for the accurate modeling of the spatial distribution of water quality parameters.

**Table 4.** Water parameter data read by task points in plans.

| Plan | Task | EC (µS/cm) | Temp (°C) | pH | DO (mg/L) | ORP (mV) |
|---|---|---|---|---|---|---|
| Plan 1 | 1 | 12,530.00 | 15.50 | 8.55 | 5.26 | 128.80 |
| Plan 1 | 2 | 12,519.00 | 15.50 | 8.56 | 5.92 | 127.10 |
| Plan 2 | 1 | 11,865.00 | 15.80 | 8.55 | 5.51 | 122.80 |
| Plan 2 | 2 | 11,345.00 | 15.70 | 8.83 | 5.12 | 126.30 |
| Plan 2 | 3 | 11,409.00 | 15.70 | 8.63 | 5.52 | 129.40 |
| Plan 3 | 1 | 11,842.00 | 15.60 | 8.38 | 4.96 | 140.30 |
| Plan 3 | 2 | 11,971.70 | 15.80 | 8.37 | 5.34 | 136.00 |
| Plan 3 | 3 | 11,740.90 | 15.70 | 8.32 | 5.91 | 128.60 |
| Plan 3 | 4 | 11,782.80 | 15.80 | 8.45 | 5.66 | 130.00 |
| Plan 3 | 5 | 11,881.30 | 15.50 | 8.38 | 5.01 | 138.20 |
| Plan 4 | 1 | 11,742.00 | 15.80 | 8.38 | 4.96 | 140.30 |
| Plan 4 | 2 | 11,741.70 | 15.70 | 8.47 | 5.24 | 136.00 |
| Plan 4 | 3 | 11,740.90 | 15.60 | 8.32 | 5.20 | 138.60 |
| Plan 4 | 4 | 11,882.80 | 15.30 | 8.35 | 5.33 | 141.70 |
| Plan 4 | 5 | 11,991.30 | 15.80 | 8.78 | 5.11 | 162.20 |
| Plan 4 | 6 | 11,742.00 | 15.80 | 8.48 | 4.76 | 144.00 |
| Plan 4 | 7 | 11,941.70 | 15.50 | 8.57 | 5.12 | 157.00 |
| Plan 4 | 8 | 11,740.90 | 15.60 | 8.40 | 4.90 | 149.90 |
| Plan 4 | 9 | 11,852.80 | 15.60 | 8.35 | 4.86 | 149.00 |
| Plan 4 | 10 | 11,861.30 | 15.60 | 8.58 | 5.01 | 141.20 |
| Plan 4 | 11 | 11,481.30 | 15.90 | 8.70 | 5.21 | 144.30 |
| Plan 4 | 12 | 11,801.30 | 15.80 | 8.45 | 5.02 | 151.00 |
| Plan 4 | 13 | 11,821.30 | 15.80 | 8.65 | 5.27 | 150.00 |
| Plan 4 | 14 | 11,521.30 | 15.90 | 8.56 | 5.01 | 139.90 |

Table 4 presents all water quality measurements collected at the task points of each navigation plan. Since there are spatial differences between the plan task points, the measurements were analyzed according to plan-level distributions, not point-based measurements. Accordingly, Figure 16 visualizes intra-plan variability and parameter distributions according to plans without establishing spatial relationships.

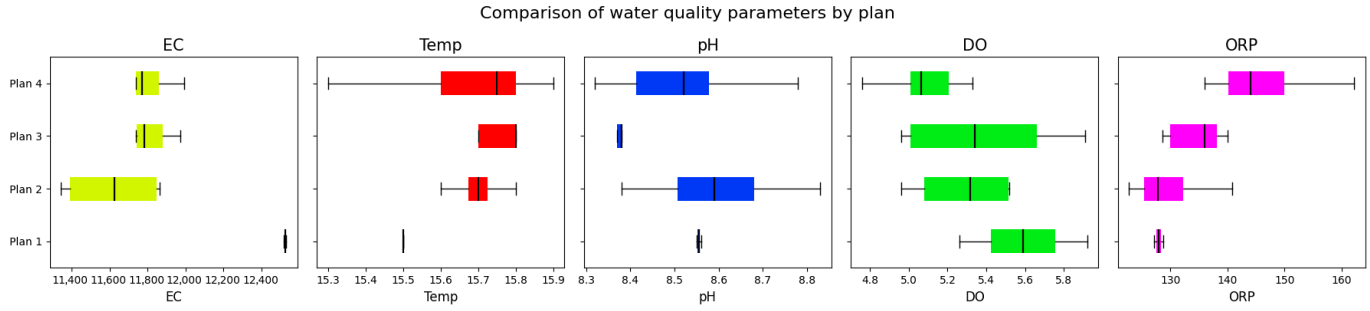


**Figure 16.** Plan-based distribution of water quality parameters measured at task points.

The AquaMIB system not only collects water quality parameters in real time but also transforms them into spatially interpretable maps. For each plan and each parameter, spatial distribution maps can be generated using four different interpolation methods (IDW, Spline, Kriging, and Natural Neighbor), and in addition, spatial distributions can be visualized through online maps. As an example, Figure 17a presents the temperature distribution generated by the IDW method, where variations between 15.3 °C and 15.9 °C are clearly visualized across the study area. Figure 17b illustrates the EC distribution, highlighting localized changes that can only be detected through spatial interpolation.

Finally, Figure 17c displays a real-time ORP heatmap produced on the web-based control panel, demonstrating the system's ability to instantly visualize monitoring results on a geographic background. Only three representative examples are presented here to illustrate the mapping approach.

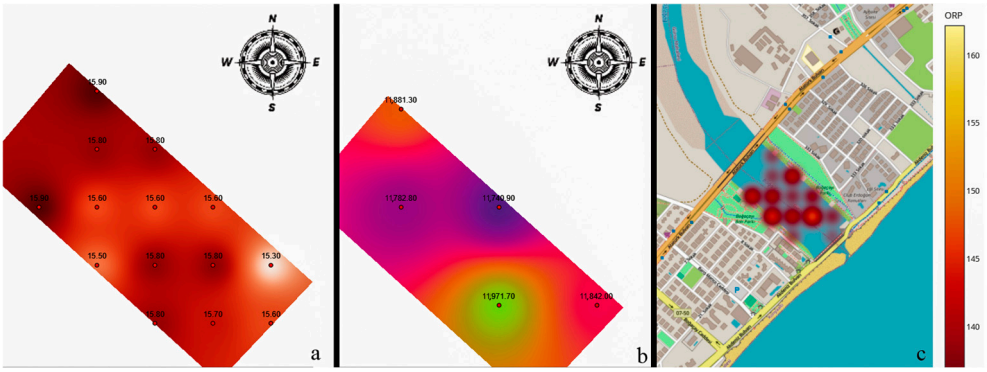


**Figure 17.** AquaMIB measurements and visualization on the control panel (**a**) Plan 4 Temperature (IDW); (**b**) Plan 3 Electrical Conductivity (IDW); (**c**) Plan 4 ORP (Realtime Heatmap).

These examples confirm that AquaMIB can convert point-based measurements into meaningful spatial outputs, supporting both scientific research and practical decision-making in aquatic environments. Examination of the maps shows that the IDW and Spline methods represent spatial distributions more clearly and continuously, whereas the Kriging and Natural Neighbor methods provide more limited representations. Data density is identified as the determining factor for these differences; in particular, the limited number of sampling points adversely affects the performance of the Kriging and Natural Neighbor methods. To validate this visual assessment with quantitative metrics, a comparative error analysis was performed using the Leave-One-Out Cross-Validation method on the highest-density dataset (Plan 4). The analysis compared the Normalized Root Mean Square Error (NRMSE) across IDW, Kriging, and Spline methods. The results quantitatively confirmed that IDW provided the most robust performance for most water quality parameters given the limited sample size ($n = 14$). For instance, in pH measurements, IDW achieved an NRMSE of 1.69%, outperforming Spline (1.82%) and Kriging (5.39%). Similarly, for Dissolved Oxygen (DO), IDW yielded the lowest error (3.20%) compared to Spline (3.71%) and Kriging (8.68%). While Spline showed a slightly better accuracy for Electrical Conductivity (1.24%) compared to IDW (1.37%), the difference was negligible. These metrics numerically support the selection of IDW as the primary interpolation method for the AquaMIB system, as it offers a superior balance between computational efficiency and accuracy for real-time mapping.

## 4. Discussion

With AquaMIB, an innovative approach to water quality monitoring is introduced, providing a system that operates autonomously and enables online data transfer. The main purpose of the system is to ensure that water quality parameters such as temperature, pH, EC, DO, and ORP can be monitored in real time and continuously over large areas, while also contributing to decision-support processes through GIS-based analysis.

The system exhibits a comprehensive structure in terms of both hardware and software. Designed in catamaran form, AquaMIB integrates multiple sensor modules, a guidance system based on a PID algorithm, LiDAR supported obstacle detection, GPS for positioning, and a digital compass for direction control. All operations including task execution, data processing, motor control, and communication are managed on a single platform using a

Raspberry Pi and the Python programming language. Real-time data transfer is achieved via SignalR, while a comprehensive web-based control panel provides an interactive interface to monitor all system movements and data instantly. Unlike alternative embedded platforms, such as Nvidia Jetson or x86 industrial PCs, the Raspberry Pi combined with Atmega 324P (Microchip Technology Inc., Chandler, AZ, USA) and Arduino Uno (Arduino S.r.l., Scarmagno, Italy) configuration offers a distinct advantage in terms of power consumption and computational efficiency. This distributed architecture allocates specific tasks to the most appropriate hardware: high-level processing and web-based communication are handled by the Raspberry Pi, while real-time sensor data acquisition is managed by the Atmega 324P, and manual control commands are processed by the Arduino Uno. This division significantly optimizes the computational load. For instance, the Remote Controller performs low-complexity tasks that do not require high processing power. By delegating real-time control tasks to Raspberry Pi, the system ensures both scalability and extended battery life for long-duration missions.

AquaMIB was initially tested in a pool environment and subsequently in a 10-hectare field study area for autonomous operation. Four different mission plans were implemented, two based on manual coordinate selection and two on spatial eld selection. Across these four plans, a total of 24 mission points were defined, all of which were successfully reached in the prescribed order. During the missions, the vehicle traveled a total of 2248.35 m, completing this distance in 34 min and 36 s with an average speed of 1.08 m/s. The difference of 80.44 m between the AquaMIB route and the linear route corresponds to a deviation of about 3.5%, which remains within acceptable limits given the natural conditions of aquatic environments and low-speed maneuvers. Studies in the literature emphasize that accumulated PID errors, overcorrections, or delays in correcting deviations when the target is distant can contribute to course oscillations [12,49]. Nevertheless, calibration of the engines, integration of dual GPS data, and use of a digital compass contributed to a route-tracking success rate of 96.5%.

Dual-positioning approach was established during the preliminary development phases. Initial pool tests revealed that standalone GPS modules frequently suffered from 'multipath effects' caused by water surface reflections, leading to instantaneous position jumps of 5–10 m. The implemented fusion algorithm (Equations (2)–(4)) addresses this by treating the GSM data as a verification layer. Instead of merely averaging two values, the algorithm functions primarily as an outlier rejection mechanism; if the deviation between sources exceeds the 3 m threshold, the erratic data point is discarded. This strategy effectively prevented the sudden heading oscillations that are typical in low-cost single-GPS systems, thereby ensuring the signal continuity and smooth trajectory observed in the autonomous mission results (Figure 13).

Of the 24 task points defined, AquaMIB reached 16 points (66.6%) within the 3 m tolerance limit, while deviations at the remaining 8 points (33.4%) exceeded this threshold. In general, the system achieved its goals with high accuracy, though larger deviations were observed at sharp turning points. Environmental factors such as currents, wind [50] and GPS error margins [51] may explain these deviations. These findings demonstrate the overall effectiveness of the system but also highlight the need for additional measures in applications requiring high precision. Integrating high-precision GNSS modules and additional environmental sensors is expected to improve reliability. For example, Jiang et al. [52] report a 50% reduction in error rates when employing high-precision GNSS navigation. AquaMIB autonomous performance was evaluated based on distance deviations in target coordinates and directional stability during navigation. Although continuous heading error logs were not stored due to the real-time operational architecture, the corrective performance of the PID controller is visually demonstrated in Figure 7. This figure illustrates the

spatial reduction of orientation offsets at sequential time steps (t1, t2, t3), confirming the vehicle's ability to stabilize its trajectory towards the target. For longer-range autonomous operations, additional performance indicators such as Cross-Track Error (XTE) and cumulative energy consumption may provide valuable insights into hydrodynamic efficiency and route-following accuracy. Although the present study focuses on task-based navigation and water quality monitoring, incorporating these metrics would further enhance performance evaluation in extended operational scenarios.

Regarding water parameter measurements, the system's accuracy is enhanced by averaging 50 repetitions per parameter. Each measurement takes about 5 s, resulting in a full cycle of five parameters in approximately 25 s. Invalid or incomplete data are automatically filtered, ensuring reliable results. The potential loss of high-frequency temporal variations was accepted to prioritize data stability and system reliability against environmental noise. This approach aligns with studies such as Kaizu et al. [53], who increased accuracy by repeating measurements, and Xing et al. [8], who eliminated erroneous turbidity data. Unlike studies that rely on single measurements [38,39,54], AquaMIB combines a multi-measurement strategy with invalid data filtering, significantly improving data reliability.

The communication performance of the system is ensured by transmitting one data packet per second via SignalR. An average packet of 105 characters is delivered with a latency as low as 130 ms, which is sufficient for real-time monitoring. This performance is consistent with the 100–200 ms latency reported for similar systems [55]. Larger data sequences are transmitted via RESTful API with a delay of about 3 s. This hybrid approach allows the system to respond instantly to critical tasks while handling high-volume data transfers efficiently. While the current system architecture successfully utilizes SignalR for high-speed real-time data transmission, future iterations targeting large-scale environmental monitoring may benefit from alternative protocols. As highlighted in recent studies on structural health monitoring [56], incorporating a Wireless Sensor Network based on the Message Queuing Telemetry Transport protocol can significantly reduce communication overhead and enhance energy efficiency. Furthermore, adopting such an architecture would improve interoperability, allowing the system to seamlessly integrate with additional stationary or mobile sensing platforms.

The web-based control panel is implemented using ASP.NET Core MVC, providing a modular and scalable infrastructure. HTML, CSS, and JavaScript support a responsive interface design, ensuring both desktop and mobile usability. Compared to earlier studies that relied on basic implementations [7,57], the AquaMIB panel offers greater flexibility, multi-device access, and enhanced user interaction.

For control, the physical remote controller has a 3 km range, while the web-based controller provides access from anywhere with internet connectivity. This dual-control structure supports manual interventions during autonomous operation, consistent with recommendations in the literature [6]. By transmitting data through two separate communication systems, the AquaMIB introduces an additional layer of operational safety and flexibility.

Interpolation methods commonly used in GIS are integrated directly into the control panel, enabling the creation of real-time spatial distribution maps. Rather than relying on post-processing in traditional GIS, this real-time capability provides immediate decision support. Consistent with findings by Liang et al. [58] and Tayyab et al. [59], IDW and Spline are shown to be less sensitive to data density compared with Kriging and Natural Neighbor, a pattern that is also observed within the AquaMIB system.

A summarized cost breakdown of the major components used in the AquaMIB prototype is presented in Table 5. The total hardware cost of the system is approximately $1576.5. As shown in the breakdown, the water quality sensor suite constitutes the largest portion of

the budget (~52%), demonstrating that the cost reduction was achieved primarily through the modular vehicle design and efficient control architecture rather than compromising sensing capability. Compared to commercial USV [60] solutions used for similar hydrographic surveys, which typically range from $15,000 to $50,000 depending on payload and autonomy levels, AquaMIB offers a significant economic advantage. By utilizing off-the-shelf electronic components and a custom-designed fiberglass hull, the proposed system reduces costs by over 90%, making autonomous water quality monitoring accessible for academic research and budget-constrained environmental management agencies.

**Table 5.** Cost breakdown of the AquaMIB system major components.

| Component Category | Hardware | Unit Cost ($) |
|---|---|---|
| Control and Computing | Raspberry Pi 4 (4 GB) + SD Card | 62 |
| | Atmega 324P | 6 |
| | Arduino Uno | 23 |
| Sensors | Water Quality Sensors (pH, EC, DO, ORP, Temp) | 822 |
| | LiDAR | 89 |
| | GPS Module | 18 |
| | Digital Compass | 4.5 |
| Propulsion and Power | Brushed Motors (x2) + ESCs + Propellers | 48 |
| | Li-Po Batteries (2x 12V 12Ah) | 92 |
| | Solar Panel & Charge Controller | 43 |
| Communication | 4G/LTE GSM Module | 83 |
| | ZigBee Modules | 31 |
| Hull | Fiberglass Hull | 102 |
| Structure | Aluminum Profiles, PCBs, Misc. | 153 |
| | Total Estimated Cost | 1576.5 |

Despite the successful validation of the AquaMIB system in generating real-time water quality maps, certain limitations inherent to the current prototype should be acknowledged. First, the maximum operational time is approximately 3 h with the current Li-Po battery configuration, which limits the system's applicability for large-scale or day-long monitoring missions without battery replacement or additional charging infrastructure. Second, while the catamaran hull design provides stability in calm to moderate waters (e.g., lakes and estuaries), the system's sensitivity to harsh weather conditions—particularly high wave amplitude and strong currents—may compromise navigation accuracy and sensor stability. Finally, the web-based control panel relies heavily on 4G/LTE coverage. Although the local ZigBee link provides a backup for short-range control, the real-time data transmission to the cloud and remote intervention capabilities may be interrupted in rural areas with weak cellular network availability. Future iterations aim to address these constraints by integrating solar-assisted propulsion for extended endurance and satellite-based communication modules for uninterrupted connectivity in remote locations.

## 5. Conclusions

In conclusion, AquaMIB represents a scalable decision-support infrastructure that can be applied to environmental monitoring, resource management, pollution detection, and modeling. With its capabilities in real-time data processing, flexible model selection, and map-based visualization, the system is by offering a different perspective valuable not only for academic research but also for environmental agencies, and water management institutions.

Future work will focus on systematic evaluation of AquaMIB under diverse natural conditions, including wind, current, waves, and variable weather, to assess impacts on mobility, stability, and energy use. Improvements may include integration of high-precision RTK-GNSS modules, wind and flow sensors for monitoring atmospheric and aquatic conditions, and enhanced LiDAR with extended scanning capabilities. Future developments will

integrate AI-driven path planning to optimize energy consumption based on real-time wind and flow sensor data, further enhancing the USV's autonomy in complex environments.

**Author Contributions:** Conceptualization, H.D.; methodology, H.D.; software, H.D.; validation, H.D.; formal analysis, H.D.; investigation, H.D.; resources, H.D.; data curation, H.D.; writing—original draft preparation, H.D., N.K.S.; writing—review and editing, H.D., N.K.S.; visualization, H.D.; supervision, N.K.S. All authors have read and agreed to the published version of the manuscript.

**Funding:** This research received no external funding.

**Institutional Review Board Statement:** Not applicable.

**Informed Consent Statement:** Not applicable.

**Data Availability Statement:** The data that support the findings of this study are available from the corresponding author upon reasonable request.

**Acknowledgments:** This work was carried out within the scope of the doctoral dissertation titled "Development of autonomous unmanned surface vehicle for online monitoring and evaluation of water parameters using GIS" at the Department of Remote Sensing and Geographic Information Systems, Graduate School of Natural and Applied Sciences, Akdeniz University. Declaration of generative AI and AI-assisted technologies in the writing process: During the preparation of this work the author(s) used Large Language Model (LLM) tool ChatGPT (GPT-4 architecture, OpenAI, San Francisco, CA, USA)to improve the readability and language of the work. After using this tool/service, the author(s) reviewed and edited the content as needed and take(s) full responsibility for the content of the publication.

**Conflicts of Interest:** The authors declare no conflicts of interest.

## Abbreviations

The following abbreviations are used in this manuscript:

| | |
|---|---|
| API | Application Programming Interface |
| AquaMIB | Autonomous Water Quality Monitoring Intelligent Boat |
| CSV | Comma-Separated Values |
| DO | Dissolved Oxygen |
| EC | Electrical Conductivity |
| GIS | Geographic Information System |
| GNSS | Global Navigation Satellite System |
| GPS | Global Positioning System |
| GSM | Global System for Mobile Communications |
| IDW | Inverse Distance Weighting |
| LiDAR | Light Detection and Ranging |
| LTE | Long-Term Evolution |
| MVC | Model–View–Controller |
| NRMSE | Normalized Root Mean Square Error |
| NN | Natural Neighbor (interpolation method) |
| ORP | Oxidation–Reduction Potential |
| PID | Proportional–Integral–Derivative (controller) |
| PPP | Point-to-Point Protocol |
| PWM | Pulse Width Modulation |
| RTK-GNSS | Real-Time Kinematic Global Navigation Satellite System |
| USV | Unmanned Surface Vehicle |
| WPMSU | Water Parameter Measurement and Sampling Unit |

## References


1. Chen, Y.; Han, D. Water quality monitoring in smart city: A pilot project. *Autom. Constr.* **2018**, *89*, 307–316. [CrossRef]
2. Bangira, T.; Matongera, T.N.; Mabhaudhi, T.; Mutanga, O. Remote sensing-based water quality monitoring in African reservoirs: Potential and limitations of sensors and algorithms. *Phys. Chem. Earth Parts A/B/C* **2024**, *134*, 103536. [CrossRef]
3. Mukta, M.; Islam, S.; Barman, S.D.; Reza, A.W.; Khan, M.S.H. IoT-based smart water quality monitoring system. In Proceedings of the 2019 IEEE 4th International Conference on Computer and Communication Systems (ICCCS), Singapore, 23–25 February 2019; IEEE: Piscataway, NJ, USA, 2019; pp. 669–673. [CrossRef]
4. Bayusari, I.; Adawiyyah, N.A.; Dwijayanti, S.; Hikmarika, H.; Husin, Z.; Suprapto, B.Y. Water quality monitoring system in autonomous underwater vehicle based on IoT. In Proceedings of the 8th International Conference on Electrical Engineering, Computer Science and Informatics, (EECSI), Semarang, Indonesia, 20–21 October 2021; IEEE: Piscataway, NJ, USA, 2021; pp. 328–334. [CrossRef]
5. Jo, W.; Hoashi, Y.; Aguilar, L.L.P.; Postigo-Málaga, M.; Garcia-Bravo, J.M.; Min, B.C. A low-cost and small USV platform for water quality monitoring. *HardwareX* **2019**, *6*, e00076. [CrossRef]
6. Stateczny, A.; Burdziakowski, P. Universal autonomous control and management system for multipurpose USV. *Pol. Marit. Res.* **2019**, *26*, 30–39. [CrossRef]
7. Dsouza, V.L.; Dsouza, S.F.; Sarosh, M.; Kukkilaya, S.; Chilimbi, V.; Fernandes, S.R. Remotely controlled boat for water quality monitoring and sampling. *Mater. Today Proc.* **2021**, *47*, 2391–2400. [CrossRef]
8. Xing, A.; Fang, J.; Gao, M.; Zhang, C. Design of an unmanned boat system for floating garbage salvage and water quality monitoring based on OneNet. *J. Phys. Conf. Ser.* **2020**, *1607*, 012062. [CrossRef]
9. Setiawan, J.D.; Ihsan, M.S.; Saputro, R.; Munadi, M.; Paryanto, P.; Alimi, S. Wireless monitoring systems for autonomous sailboat. *J. Phys. Conf. Ser.* **2022**, *2193*, 012050. [CrossRef]
10. DeepChand; Khan, N.A.; Saxena, P.; Goyal, S.K. Assessment of supply water quality using GIS tool for selected locations in Delhi —A Case Study. *Air Soil Water Res.* **2022**, *15*, 1–9. [CrossRef]
11. Yanes Luis, S.; Gutiérrez-Reina, D.; Toral Marín, S. A dimensional comparison between evolutionary algorithm and deep reinforcement learning methodologies for autonomous surface vehicles with water quality sensors. *Sensors* **2021**, *21*, 2862. [CrossRef]
12. Si, H.; Zhang, N.; Liu, Y.; Jing, G.; Ren, Y.; Yang, P. Application and field comparison of water quality monitors in unmanned surface vehicle. In Proceedings of the IEEE 16th International Conference on Electronic Measurement and Instruments, Harbin, China, 9–11 August 2023; IEEE: Piscataway, NJ, USA, 2023; pp. 52–56. [CrossRef]
13. Kassuba, Z.; Goldenbogen, M.; Jannetta, C.; Vicent, X.; Sarda, E.I. Development of a water quality monitoring system on a USV. In Proceedings of the OCEANS 2024, Halifax, NS, Canada, 23–26 September 2024; IEEE: Piscataway, NJ, USA, 2024; p. 18. [CrossRef]
14. Zhartybayeva, M.; Serik, N.; Nurzhanova, A.; Rakhimov, R.; Tulegenova, S. Development of an integrated approach to the analysis and forecast of hydrographic and bathymetric data of water bodies and tailings ponds. *East.-Eur. J. Enterp. Technol.* **2024**, *127*, 36–46. [CrossRef]
15. Abidin, M.I.Z.; Ismail, K.; Zawawi, F.M.; Elabd, O.E.S.A.; Abdelmetaal, A.; Nor, N.S.M. Evaluation of autonomous navigation and path accuracy for unmanned surface vehicles using IMU sensor and GPS data. *J. Transp. Syst. Eng.* **2024**, *14*, 14–20. [CrossRef]
16. Aparicio-Lastiri, L.M.; Cárdenaz-Velázquez, J.I.; Antonio-Yañez, E.D.; Núñez-Cruz, R.S. Measurement of water quality using an unmanned surface vehicle. In Proceedings of the XXV Robotics Mexican Congress (COMRob), Xalapa/Veracruz, Mexico, 15–17 November 2023; IEEE: Piscataway, NJ, USA, 2023; pp. 13–18. [CrossRef]
17. Chen, W.; Hao, X.; Yan, K.; Lu, J.; Liu, J.; He, C.; Zhou, F.; Xu, X. Mobile water quality monitoring system based on LPWAN and unmanned surface vehicle. *Wirel. Commun. Mob. Comput.* **2021**, *2021*, 1609612. [CrossRef]
18. Ryu, J.H. Prototyping a low-cost open-source USV for real-time water quality monitoring. *HardwareX* **2022**, *12*, e00369. [CrossRef] [PubMed]
19. Tran, H.D.; Nguyen, N.T.; Cao, T.N.T.; Gia, L.X.; Ho, K.; Nguyen, D.D.; Pham, B.T.; Truong, V.N. Unmanned surface vehicle for automatic water quality monitoring. *E3S Web Conf.* **2024**, *496*, 03005. [CrossRef]
20. Vargas, S.M.; Vitale, A.J.; Genchi, S.A.; Nogueira, S.F.; Arias, A.H.; Perillo, G.M.; Siben, A.; Delrieux, C.A. Monitoring multiple parameters using a low-cost open-source platform. *HardwareX* **2023**, *16*, e00492. [CrossRef] [PubMed]
21. Hussein, A.K.; Kadhim, N.A.; Jaber, A.S.; Abojassim, A.A. Water quality index for surface water assessment using GIS techniques. *IOP Conf. Ser. Mater. Sci. Eng.* **2020**, *928*, 072023. [CrossRef]
22. Venkataraman, T.; Manikumari, N. Spatial distribution of water quality parameters using GIS. *Int. J. Innov. Technol. Explor. Eng.* **2019**, *9*, 3936–3941. [CrossRef]
23. Kurunc, A.; Ersahin, S.; Sonmez, N.K.; Kaman, H.; Uz, I.; Uz, B.Y.; Aslan, G.E. Seasonal changes of spatial variation of some groundwater quality variables in a large irrigated coastal Mediterranean region of Turkey. *Sci. Total Environ.* **2016**, *554*, 53–63. [CrossRef]

24. Khorrami, B.; Gunduz, O. Improved spatial variation pattern based on geostatistical interpolation techniques for monthly average rainfall: An example from Izmir, Turkey. In Proceedings of the 10th National Hydrology Congress, Mugla, Turkey, 9–12 October 2019; p. 113.
25. Yang, X.; Xie, X.; Liu, D.L.; Ji, F.; Wang, L. Spatial interpolation of daily rainfall data for local climate impact assessment over Greater Sydney region. *Adv. Meteorol.* **2015**, *2015*, 563629. [CrossRef]
26. Khouni, I.; Louhichi, G.; Ghrabi, A. GIS-based IDW interpolation to assess surface water quality. *Environ. Technol. Innov.* **2021**, *24*, 101892. [CrossRef]
27. Murphy, R.R.; Curriero, F.; Ball, W.P. Comparison of spatial interpolation methods for water quality evaluation in the Chesapeake Bay. *J. Environ. Eng.* **2010**, *136*, 160–171. [CrossRef]
28. Tanjung, M.; Syahreze, S.; Rushdi, M. Comparison of interpolation methods based on Geographic Information System (GIS) in the spatial distribution of seawater intrusion. *J. Nat.* **2020**, *20*, 24–30. [CrossRef]
29. Ferchichi, H.; St-Hilaire, A.; Ourda, T.B.M.J.; Levesque, B. Impact of future coastal water temperature scenarios on the risk of pathogenic Vibrio marine bacteria. *Estuar. Coast. Shelf Sci.* **2021**, *250*, 107094. [CrossRef]
30. Benzouai, S.; Houma, F.; Belkessa, R.; Zerouali, K.; Boufeniza, R.L. Using GIS for spatiotemporal assessment of physicochemical parameters in the Bay of Algiers. In Proceedings of the IEEE International Geoscience and Remote Sensing Symposium, Milan, Italy, 26–31 July 2015; IEEE: Piscataway, NJ, USA, 2015; pp. 4526–4529. [CrossRef]
31. Muthulakshmi, A.; Natesan, U.; Ferrer, V.A.; Deepthi, K.; Venugopalan, V.P.; Narasiman, S.V. GIS based spatial distribution of Temperature and Chlorophyll-a along Kalpakkam, southeast coast of India. *Int. J. Eng. Res. Appl.* **2015**, *5*, 121–126.
32. Maliqi, E.; Penev, P. Spatial representation of surface water monitoring and its assessment using geostatistical and non-geostatistical techniques in GIS. *Geod. Cartogr.* **2019**, *45*, 177–189. [CrossRef]
33. Isa, A.R.M.; Yusof, I.M.; Rahman, R.A. Lake water quality assessment through GIS-based interpolation method: A case study of Beris Dam, Kedah, Malaysia. *Trends Sci.* **2024**, *21*, 116. [CrossRef]
34. Lateef, Z.Q.; Al-Madhhachi, A.S.T.; Sachit, D.E. Evaluation of water quality parameters in Shatt AL-Arab, Southern Iraq, using spatial analysis. *Hydrology* **2020**, *7*, 79. [CrossRef]
35. O'Donnell, D.; Rushworth, A.; Bowman, A.W.; Scott, M.E.; Hallard, M. Flexible regression models over river networks. *J. R. Stat. Soc. Ser. C Appl. Stat.* **2014**, *63*, 47–63. [CrossRef] [PubMed]
36. Sheehan, K.R.; Welsh, S.A. An interpolation method for stream habitat assessments. *N. Am. J. Fish. Manag.* **2009**, *29*, 1–9. [CrossRef]
37. Kawahito, S.; Seo, M.W. Noise reduction effect of multiple-sampling-based signal-readout circuits for ultra-low-noise CMOS image sensors. *Sensors* **2016**, *16*, 1867. [CrossRef] [PubMed]
38. Chang, H.C.; Hsu, Y.L.; Hung, S.S.; Ou, G.R.; Wu, J.R.; Hsu, C. Autonomous water quality monitoring and water surface cleaning for unmanned surface vehicle. *Sensors* **2021**, *21*, 1102. [CrossRef]
39. Arko, S.R.; Issa, R.B.; Das, M.; Rahman, M.S. Autonomous surface vehicle for real-time monitoring of water bodies in Bangladesh. In Proceedings of the Global Oceans 2020, Biloxi, MS, USA, 5–30 October 2020; IEEE: Piscataway, NJ, USA, 2021; p. 17. [CrossRef]
40. Wang, W.; Liu, Y.; Chen, Y.; Li, C. Optimization-based duty cycle allocation for a five-leg inverter to drive two electric motors. *IEEE Trans. Power Electron.* **2023**, *38*, 11327–11337. [CrossRef]
41. Villa, J.; Aaltonen, J.; Koskinen, K. Path-following with LiDAR-based obstacle avoidance of an unmanned surface vehicle in harbor conditions. *IEEE/ASME Trans. Mechatron.* **2020**, *25*, 1812–1820. [CrossRef]
42. Theobald, D.M.; Stevens, D.L.; White, D.; Urquhart, N.S.; Olsen, A.R.; Norman, J.B. Using GIS to generate spatially balanced random survey designs for natural resource applications. *Environ. Manag.* **2007**, *40*, 134–146. [CrossRef] [PubMed]
43. Balbuena, J.; Quiroz, D.; Song, R.; Bucknall, R.; Cuellar, F. Design and implementation of an USV for large bodies of fresh waters at the highlands of Peru. In Proceedings of the OCEANS 2017, Anchorage, AK, USA, 18–21 September 2017; IEEE: Piscataway, NJ, USA, 2017; pp. 1–8.
44. Shepard, D. A two-dimensional interpolation function for irregularly spaced data. In Proceedings of the 23rd ACM National Conference, Las Vegas, NV, USA, 27–29 August 1968; ACM Press: New York, NY, USA, 1968; pp. 517–524. [CrossRef]
45. Chiles, J.P.; Delfiner, P. *Geostatistics: Modeling Spatial Uncertainty*; John Wiley and Sons: Hoboken, NJ, USA, 2012. [CrossRef]
46. Franke, R. Smooth interpolation of scattered data by local thin plate splines. *Comput. Math. Appl.* **1982**, *8*, 273–281. [CrossRef]
47. Sambridge, M.; Braun, J.; McQueen, H. Geophysical parametrization and interpolation of irregular data using natural neighbours. *Geophys. J. Int.* **1995**, *122*, 837–857. [CrossRef]
48. U.S. Ocean Acidification Interagency Working Group. *Global Positioning System (GPS) Standard Positioning Service Performance Analysis Report*; National Oceanic and Atmospheric Administration: Washington, DC, USA, 2014.
49. Sun, H.; Wang, L.; Li, D.; Wang, C. AUV plane tracking control algorithm. *J. Phys. Conf. Ser.* **2025**, *3004*, 012089. [CrossRef]
50. Lobo, F.; Grael, D.; Oliveira, H.; Villas, L.; Almehmadi, A.; El-Khatib, K. Cooperative localization improvement using distance information in vehicular ad hoc networks. *Sensors* **2019**, *19*, 5231. [CrossRef]

51. Zhu, K.; Deng, C.; Zhang, F.; Kang, H.; Wen, Z.; Guo, G. A multi-source fusion navigation system to overcome GPS interruption of unmanned ground vehicles. *IEEE Access* **2023**, *11*, 61070–61081. [CrossRef]
52. Jiang, X.; Kuroiwa, T.; Cao, Y.; Sun, L.; Zhang, H.; Kawaguchi, T.; Hashimoto, S. Enhanced pure pursuit path tracking algorithm for mobile robots optimized by NSGA-II with high-precision GNSS. *Sensors* **2025**, *25*, 745. [CrossRef]
53. Kaizu, Y.; Iio, M.; Yamada, H.; Noguchi, N. Development of unmanned airboat for water-quality mapping. *Biosyst. Eng.* **2011**, *109*, 338–347. [CrossRef]
54. Shuo, J.; Yonghui, Z.; Wen, R.; Kebin, T. Unmanned autonomous cruise ship for water quality monitoring. In Proceedings of the ICCSEC, Dalian, China, 25–27 December 2017; IEEE: Piscataway, NJ, USA, 2018; pp. 700–703. [CrossRef]
55. Microsoft Azure. Performance Guide for Azure SignalR Service. Available online: https://learn.microsoft.com/en-us/azure/azure-signalr/signalr-concept-performance (accessed on 20 January 2026).
56. Bono, F.M.; Polinelli, A.; Radicioni, L.; Benedetti, L.; Castelli-Dezza, F.; Cinquemani, S.; Belloli, M. Wireless Accelerometer Architecture for Bridge SHM: From Sensor Design to System Deployment. *Future Internet* **2025**, *17*, 29. [CrossRef]
57. Cao, H.; Guo, Z.; Gu, Y.; Zhou, J. Design and implementation of unmanned surface vehicle for water quality monitoring. In Proceedings of the IEEE IAEAC, Chongqing, China, 12–14 October 2018; IEEE: Piscataway, NJ, USA, 2018; pp. 1574–1577. [CrossRef]
58. Liang, Q.; Nittel, S.; Whittier, J.C.; De Bruin, S. Real-time IDW interpolation for streaming sensor data. *Trans. GIS* **2018**, *22*, 1179–1204. [CrossRef]
59. Tayyab, M.; Aslam, R.A.; Farooq, U.; Ali, S.; Khan, S.N.; Iqbal, M.; Khan, M.I.; Saddique, N. Comparative study of geospatial techniques for interpolating groundwater quality data in agricultural areas of Punjab, Pakistan. *Water* **2024**, *16*, 139. [CrossRef]
60. De Andrade, E.M.; Sales, J.S., Jr.; Fernandes, A.C. Operative Unmanned Surface Vessels (USVs): A Review of Market-Ready Solutions. *Automation* **2025**, *6*, 17. [CrossRef]


**Disclaimer/Publisher's Note:** The statements, opinions and data contained in all publications are solely those of the individual author(s) and contributor(s) and not of MDPI and/or the editor(s). MDPI and/or the editor(s) disclaim responsibility for any injury to people or property resulting from any ideas, methods, instructions or products referred to in the content.